ELECTRONIC SUPPLEMENTARY INFORMATION

A molecular dynamics study of nonlinear spectra and structure of charged (101) quartz/water interface

Konstantin S. Smirnov

Univ. Lille, CNRS, UMR 8516 – LASIRe – Laboratoire Avancé de Spectroscopie pour les Interactions la Réactivité et l'Environnement, F-59000 Lille, France

S1 Computational details

S1.1 Nonbonded interatomic interaction potentials.

The nonbonded interatomic interactions were described by the sum of Lennard–Jones (12–6) and electrostatic potentials

$$E_{NB}^{(ij)}(r) = D_0^{(ij)}\left[\left(\frac{R_0^{(ij)}}{r}\right)^{12} - 2\left(\frac{R_0^{(ij)}}{r}\right)^{6}\right] + \frac{q_i q_j}{r} \tag{S1}$$

where i and j denote two atoms separated by a distance r, and R_0, D_0 and q are parameters whose values are given in Table S1.

Table S1: Parameters of interatomic potential functions (S1).

Atom[a]	Ow[b]	Hw[b]	Oh[c]	H[c]	Si[c]	Ob[c]	Six[c]	Ox[c,d]	Na[e]	Cl[e]
$q, \lvert e^- \rvert$	−0.82	+0.41	−0.675	+0.40	+1.1	−0.55	+0.725	−0.90	+1.0	−1.0
R_0, Å	3.5532	1.0	3.47	1.085	4.15	3.47	4.15	3.5532	2.424	5.422
D_0, kcal/mol	0.1554	0.0	0.122	0.015	0.093	0.054	0.093	0.1554	0.3526	0.0128

[a] Atom notation: Ow – water oxygen, Hw – water hydrogen, Oh – hydroxyl oxygen, H – hydroxyl hydrogen, Si – silicon, Ob – oxygen of siloxane bridges, Six – silicon of SiO^- groups, Ox – oxygen of SiO^- groups, Na – sodium, Cl – chlorine;
[b] ref. 1;
[c] ref. 2;
[d] vdW parameters were set to those of Ow kind, see Section 2 of the main article;
[e] ref. 3.

S1.2 Structural descriptors.

Structural organization of silica/water interface was characterized by a number of quantities. First, profiles of relative density $\rho^*(z)$ and of orientational order parameter $S_2(z)$ for the molecular dipole and the HH vector along the direction perpendicular to the surface (Cartesian z-axis) were computed. These quantities are given by

$$\rho^*(z) = \rho(z)/\rho_0 \tag{S2}$$

$$S_2(z) = \left\langle \frac{1}{N_z}\sum_{i=1}^{N_z} P_2(\cos\theta_i)\right\rangle, \tag{S3}$$

where ρ_0 is the density of bulk liquid water, $\cos\theta_i$ is the cosine between the vector and the z-axis, $P_2()$ is the second-order Legendre polynomial and N_z is a number of molecules in with CoM z-coordinate from

z to $z + \Delta z$. $S_2 = 1$ indicates the parallel-to-axis orientation, $S_2 = -0.5$ corresponds to a mean vector orientation perpendicular to the z-axis, and $S_2 = 0$ results from a random orientation of the vector with respect to the axis.

In addition to the $S_2(z)$ profiles, the orientation of water molecules in the interfacial region was described with a joint probability density distribution $P(u_1, u_2, \mathcal{Z})$ defined as[4]

$$P(u_1, u_2, \mathcal{Z}) = \frac{1}{N_\mathcal{Z}} \langle \sum_{i \in \mathcal{Z}} \delta(u_1 - \cos\phi_1^{(i)}) \cdot \delta(u_2 - \cos\phi_2^{(i)}) \rangle, \tag{S4}$$

where $\cos\phi_k^{(i)}$ ($k = 1, 2$) is the cosine of angle between the k-th OH bond vector of molecule i and the z-axis and the sum in (S4) runs over molecules in a region $\mathcal{Z}$. The normalization factor $N_\mathcal{Z}$ is given by

$$\int_{-1}^{1} P(u_1, u_2, \mathcal{Z})\, du_1 du_2 = 1. \tag{S5}$$

The analysis was perfomed for a quantity $\widetilde{P}(u_1, u_2, \mathcal{Z})$ given by

$$\widetilde{P}(u_1, u_2, \mathcal{Z}) = P(u_1, u_2, \mathcal{Z}) / P(u_1, u_2, \infty), \tag{S6}$$

wherea $P(u_1, u_2, \infty)$ stands for the distribution (S4) in an isotropic medium taken as bulk liquid water.

Network of intermolecular H-bonds was characterized by a joint probability density distribution $Q(r, u, \mathcal{Z})$ given by[5]

$$Q(r, u, \mathcal{Z}) = \langle \sum_{i \in \mathcal{Z}} \delta(r - R_{\mathrm{DA}}^{(i)}) \cdot \delta(u - \cos\psi^{(i)}) \rangle, \tag{S7}$$

where $R_{\mathrm{DA}}^{(i)}$ and $\cos\psi^{(i)}$ are the H-bond donor–acceptor (DA) distance and the cosine of angle between the DA vector and the z-axis, respectively. The sum in (S7) runs over donor atoms with the z-coordinate lying in the region $\mathcal{Z}$. Hydrogen bonds were identified using geometric criteria[6].

S1.3 Nonlinear spectra.

Nonlinear spectra of interfacial water were obtained with the time correlation function (TCF) approach[7]. Following the approach, the pqr component of the resonant (R) part of the frequency-dependent second-order nonlinear susceptibility tensor $\boldsymbol{\chi}^{(2)}(\omega)$ is given by

$$\chi_{pqr}^{(2),R}(\omega) = \frac{i\omega}{k_B T} \int_0^\infty dt\, e^{i\omega t} \langle M_r(0) \cdot A_{pq}(t) \rangle, \tag{S8}$$

where M_r and A_{pq} are the r and pq elements of the system dipole $\mathbf{M}$ and polarizability $\mathbf{A}$, respectively. Experimentally, the most information is extracted from the analysis of sum-frequency generation spectra measured with the ssp polarization combination, that is the s- and p-polarized visible and infrared pulses, respectively, and the s-polarized sum-frequency radiation. The ssp spectrum in the work is obtained as the average of spectra of the xxz and yyz elements of the $\boldsymbol{\chi}^{(2),R}$ tensor (see below). Hereafter, the corresponding quantity is denoted as $\chi_{\parallel\parallel\perp}^{(2),R}(\omega)$ (the $\parallel$ and $\perp$ symbols respectively designate the x or y, and z components). The spectrum is computed using the convention where the z-axis is directed toward the surface (see Fig. 1 of the main article).

The dipole moment $\mathbf{M}$ and polarizability tensor $\mathbf{A}$ of the liquid phase are obtained as

$$\mathbf{M} = \sum_m \boldsymbol{\mu}_m \tag{S9}$$

$$\mathbf{A} = \sum_m \boldsymbol{\alpha}_m, \tag{S10}$$

where $\boldsymbol{\mu}_m$ and $\boldsymbol{\alpha}_m$ stand for dipole moment and polarizability tensor of molecule m, respectively. Therefore, the TCF in (S8) corresponding to the $\chi^{(2),R}_{\parallel\parallel\perp}$ element of $\boldsymbol{\chi}^{(2),R}$ is given by[8–10]

$$C_{\parallel\parallel\perp}(t) = \frac{1}{2}\Big(\langle\sum_m \mu_{\perp,m}(0)\cdot a_{\parallel\parallel,m}(t)\rangle + \langle\sum_m \mu_{\perp,m}(0)\cdot\sum_{n\neq m} a_{\parallel\parallel,n}(t)\rangle\Big), \tag{S11}$$

where the first and second terms in (S11) are intramolecular (self) and intermolecular (cross) parts of the TCF, respectively. The calculation of the cross TCF in (S11) was restricted to molecules n within a sphere of 5.5 Å radius centered at the molecule m. A contribution of molecules of bulk region to the TCFs (S11) was attenuated[9–11] by multiplying the dipole $\mu_{\perp,m}(0)$ by a damping function $g(z_m)$

$$\mu'_{\perp,m}(0) = g(z_m(0))\mu_{\perp,m}(0), \tag{S12}$$

with $z_m(0)$ being the z-coordinate of the molecule m at $t = 0$; $\mu'_{\perp,m}(0)$ replaces $\mu_{\perp,m}(0)$ in (S11). The $g(z)$ function has the form

$$g(z) = \frac{1}{2}\mathrm{sign}(z)\big(\tanh(s(|z| - z_0)) + 1\big), \tag{S13}$$

where $g(z_0) = 1/2$ and parameter s determines the width of transition region. The value $s = 8.8$ Å^{-1} used in the work yields a width of 0.25 Å for the $0.1 - 0.9$ region. The `sign()` function in (S13) prevents the dipole $M_\perp$ from the cancellation because of the symmetry of the water slab with respect to $z = 0$. The TCF (S11) was computed on a length $L = 2048$ points (8.192 ps) and multiplied by a Hann apodization function of width $L/2$ prior to performing the Laplace-Fourier transform. The resulting spectra were smoothed by using a Gaussian filter with parameter σ equal to twice the frequency-step in the spectra (4.07 cm^{-1}). To estimate statistical uncertainty of the spectra calculation, a bootstrap sampling of 500 samples was performed for the dataset of 50 computed spectra. The uncertainties were subsequently used to obtain those of derived quantities.

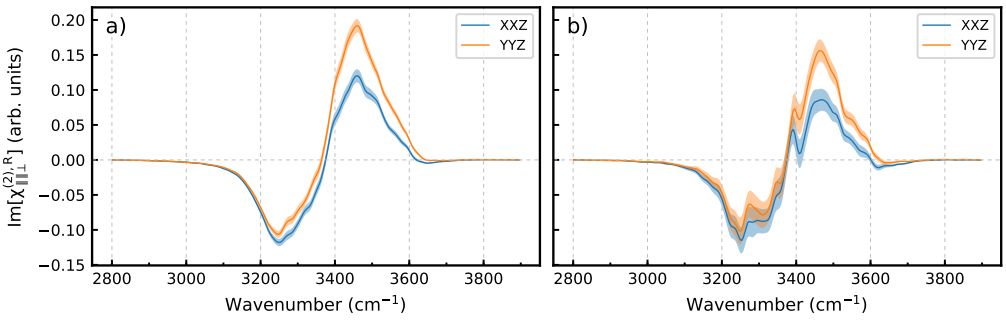

Figure S1: Im[$\chi^{(2),R}_{xxz}$] and Im[$\chi^{(2),R}_{yyz}$] spectra computed for the pH3@0.25M system: a) – spectrum of BIL, b) – spectrum of total interfacial region. Colored area represents the standard error.

Figure S1 presents Im$\chi^{(2),R}_{xxz}$ and $\chi^{(2),R}_{yyz}$ spectra computed the (101) α-quartz/water interface at pH = 3 and 0.5 M ionic strength. Qualitatively, the xxz and yyz spectra behave very similar. As the positive band stems from OH oscillators directed towards the surface, the difference of intensities of the band in the BIL spectra is readily attributable to the particular morphology of the (101) surface that features rows of silanols groups along the y direction (see Fig. 1 of the main article).

S1.4 Spectrum of third-order susceptibility of bulk water.

The dipole $\boldsymbol{\mu}_m$ of molecule m can be written as

$$\boldsymbol{\mu}_m = \boldsymbol{\mu}^{(o)}_m + \boldsymbol{\mu}^{(i)}_m, \tag{S14}$$

where the first and the second term are the permanent and induced dipoles, respectively. Then, the TCF in (S8) can be rewritten as

$$C_{pqr}(t) = \langle M_r(0) \cdot A_{pq}(t) \rangle = \langle M_r^{(o)}(0) \cdot A_{pq}(t) \rangle + \langle M_r^{(i)}(0) \cdot A_{pq}(t) \rangle \tag{S15}$$

with $M_r^{(o)}$ and $M_r^{(i)}$ being the permanent (o) and induced (i) dipoles of the system, respectively, obtained by summing the corresponding molecular quantities (S9). If an electric field is applied to the system along an s-axis ($s = x, y, z$), the induced term in (S15) can be recast into

$$C_{pqr}^{(i)}(t) = \langle A_{rs}(0) \cdot A_{pq}(t) \rangle \, E_s \tag{S16}$$

where E_s is the field component along the axis. A $pqrs$ element of third-order susceptibility $\chi^{(3)}$ is given by

$$\chi_{pqrs}^{(3)} = \partial \chi_{pqr}^{(2)} / \partial E_s, \tag{S17}$$

and using (S8) and (S16), one readily obtains an expression for $\chi_{pqrs}^{(3),R}$ as

$$\chi_{pqrs}^{(3),R}(\omega) = \frac{i\omega}{k_B T} \int_0^\infty dt \, e^{i\omega t} \langle A_{rs}(0) \cdot A_{pq}(t) \rangle \tag{S18}$$

or with the use of (S10)

$$\chi_{pqrs}^{(3),R}(\omega) = \sum_m \left[\frac{i\omega}{k_B T} \int_0^\infty dt \, e^{i\omega t} \langle \alpha_{rs,m}(0) \cdot \left(\sum_n \alpha_{pq,n}(t) \right) \rangle \right]. \tag{S19}$$

One can further split (S19) into the sum of self and cross terms, similarly to (S11). Note that the quantity in the square brackets in (S19) can be associated with the corresponding element of third-order molecular polarizability. It is worthy of noting that the above development is closely related to that in refs. 12–15, cf. eqn (1) of ref. 15.

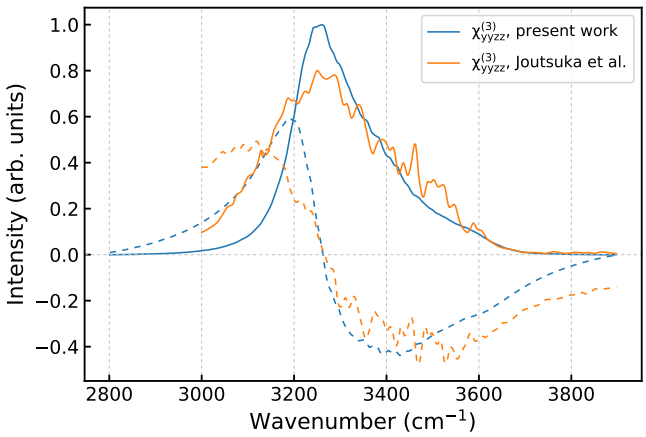

Figure S2: Calculated spectrum of the $yyzz$ element of $\chi^{(3),R}$ susceptibility of bulk water. Blue – present work, orange – digitized from Fig. 1a of ref. 16. Full and dashed lines denote the imaginary and real parts, respectively.

Figure S2 displays the spectrum of $\chi_{yyzz}^{(3),R}$ element for bulk liquid water computed with (S19) and compares it with the spectrum obtained in ref. 16. One sees a good agreement between the two spectra with differences readily explainable by different water models.

S2 Complementary results

S2.1 Vibrational spectra of isotopically diluted water.

Figure S3 shows the OH bond stretching region of power spectrum of H atoms in an H_2O molecule diluted in bulk D_2O and of the atoms in normal water. The simulated system consisted of 500 molecules and represented liquid water at $\rho^* = 1$ and a temperature of 293 K. The strong similarity between the two spectra suggests a minor effect of intermolecular vibrational coupling on the spectrum.

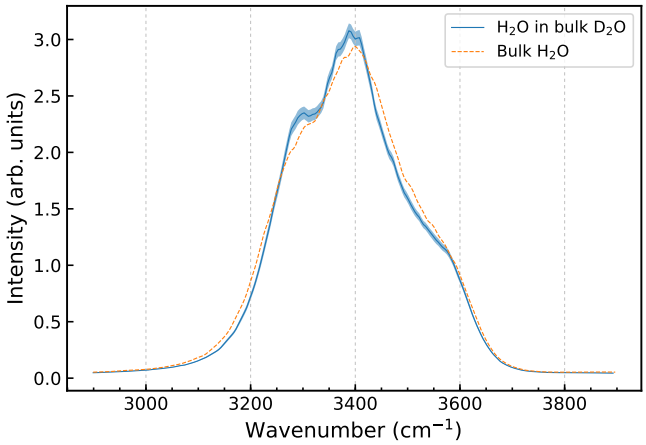

Figure S3: Power spectrum of H atoms of an H_2O molecule diluted in D_2O compared to the spectrum of H atoms in normal water. Colored area represents the standard error.

S2.2 Vibrational spectra of surface silanol groups.

Figure S4 displays the OH bond stretching region of power spectrum of H atoms of silanol groups on the (101) quartz surface for two interfacial systems. The power spectrum of H atoms in H_2O molecules of bulk liquid water is given for comparison.

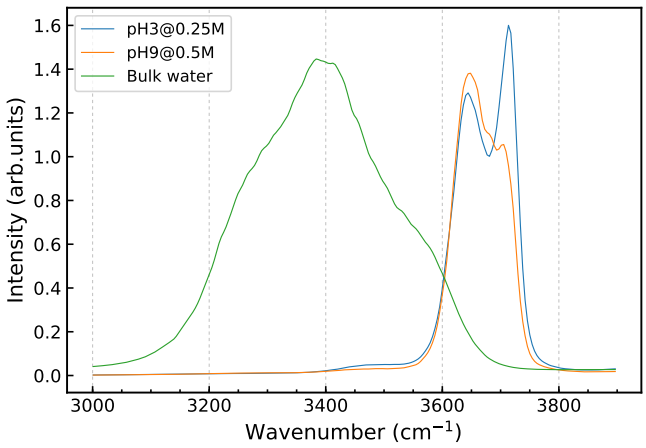

Figure S4: Power spectra of H atoms of OH groups of the (101) quartz surface in the region of the O–H stretching vibration for two interfacial systems. A power spectrum oh H atoms of water molecules in bulk liquid water is given for comparison.

S2.3 Breakdown of $\mathrm{Im}[\chi^{(2),R}_{\parallel\parallel\perp}]$ spectra of BIL at the 0.5 M ionic strength.

Figure S5 presents the breakdown of the $\mathrm{Im}[\chi^{(2),R}_{\parallel\parallel\perp}]$ spectra of BIL of quartz/water interface into the orientational and induced components for the 0.5 M NaCl solution.

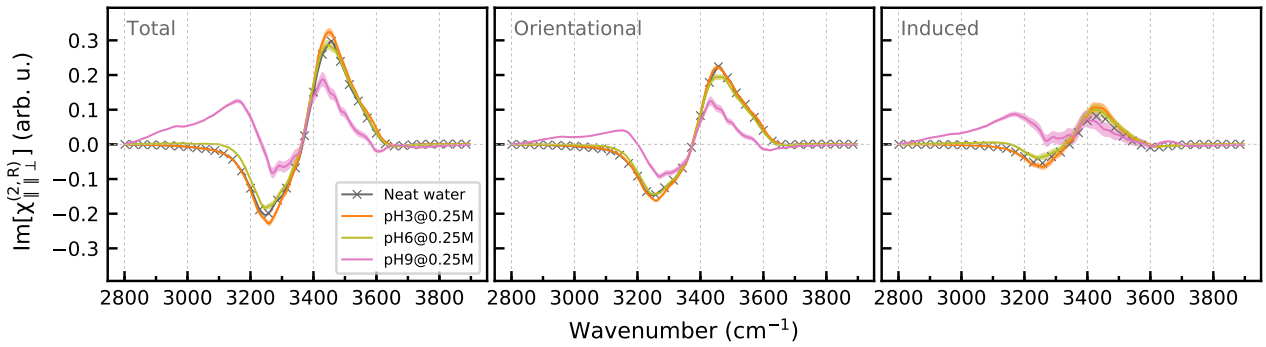

Figure S5: Breakdown of the $\mathrm{Im}[\chi^{(2),R}_{\parallel\perp}]$ spectra of BIL of (101) α-quartz/water interfaces into the orientational and induced components at the 0.5 M electrolyte concentration. The corresponding spectra of neutral surface/neat water interface are given for completeness. Colored areas represent the standard error.

S2.4 Orientation maps of OH bonds in BIL at the 0.5 M ionic strength

Figure S6 shows the $\widetilde{P}(u_1, u_2, \mathcal{Z})$ maps computed for water in BIL of the quartz/water interface for different pH values at the 0.5 M ionic strength. The patterns are essentially the same as for the 0.25 M electrolyte solution, cf Figure 12 of the main article.

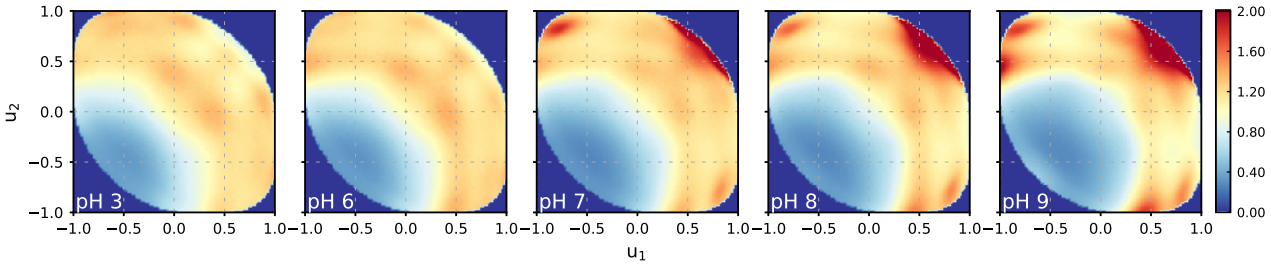

Figure S6: $\widetilde{P}(u_1, u_2, \mathcal{Z})$ maps for H_2O molecules in BIL of the (101) α-quartz/water interface at different pH values for the 0.5 M ionic strength.

S2.5 Orientation maps of OH bonds in BIL and DL of silica/neat water interface.

Figure S7 displays the $\widetilde{P}(u_1, u_2, \mathcal{Z})$ maps computed for water in BIL and DL of the quartz/neat water interface. Map in the BIL region (Fig. S7a) is very similar to those in BIL of quartz/electrolyte solutions systems for pH < 7 (cf Fig. 12 of the main article and Fig. S6).

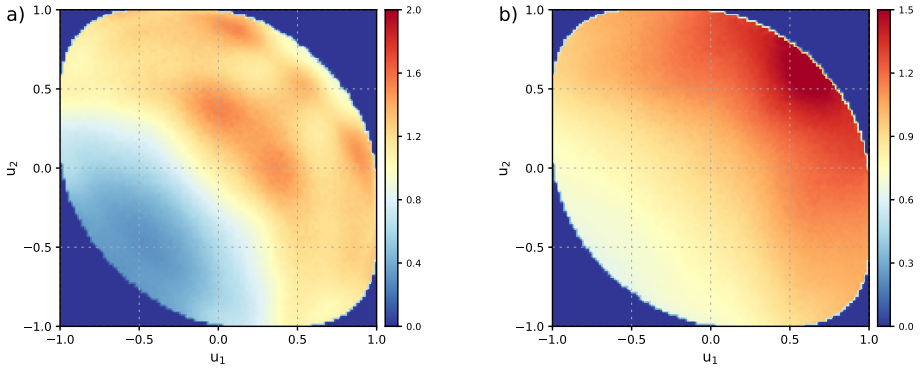

Figure S7: $\widetilde{P}(u_1, u_2, \mathcal{Z})$ maps for H_2O molecules in BIL (a) and DL (b) of the (101) α-quartz/neat water interface.

Map in DL of the quartz/neat water interface shows a slightly higher intensity of the pattern com-

pared to the maps in the diffuse layer of the electrolyte solutions (cf Fig. 13 of the main article). This feature is in line with a higher intensity of the orientational $\mathrm{Im}[\chi^{(2),R}_{\|\|\perp}]$ DL spectra for the quartz/neat water interface compared to the spectra of the quartz/NaCl solution interfaces (Fig. 8 of the main article).

S2.6 Orientation maps of H-bonding network in water on neutral and charged (101) quartz surfaces.

Figure S8 displays the $Q(r, u, \mathcal{Z})$ (S7) maps computed for water in BIL of the quartz/neat water interface and in different interfacial regions of the pH9@0.5M system. The comparison of the maps in BIL of the two systems shows that the surface charge and the formation of Helmholtz layer of adsorbed Na^+ ions suppress intermolecular H-bonds parallel to the surface (at $u \approx 0$). A mean donor-acceptor distance remains independent of distance from the surface and is unaffected by the surface charge.

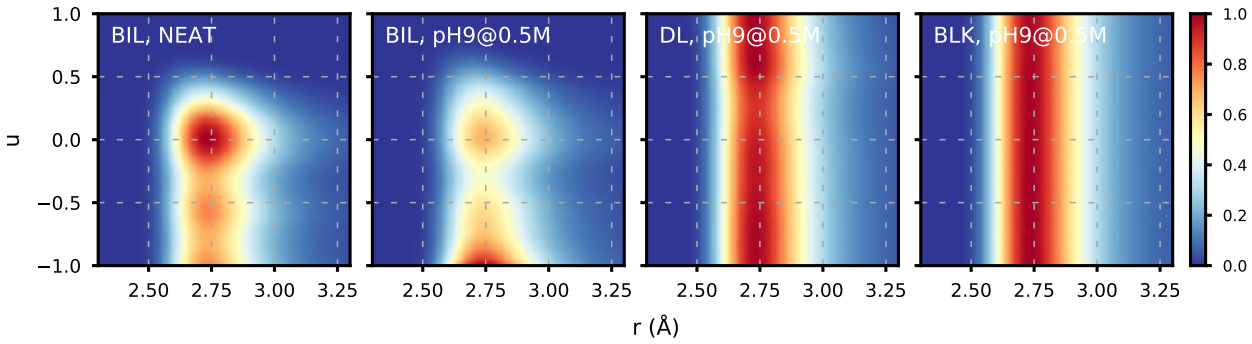

Figure S8: $Q(r, u, \mathcal{Z})$ maps for H_2O molecules in BIL of the quartz/neat water interface and the BIL, DL and bulk regions of the pH9@0.5M system.

S2.7 z-profiles of water structural characteristics in all systems

Profiles of the density ρ^* and order parameters S_2 along the z-axis for all studied systems are shown in Figure S9. Inspection of the data supports the conclusions presented in the main article.

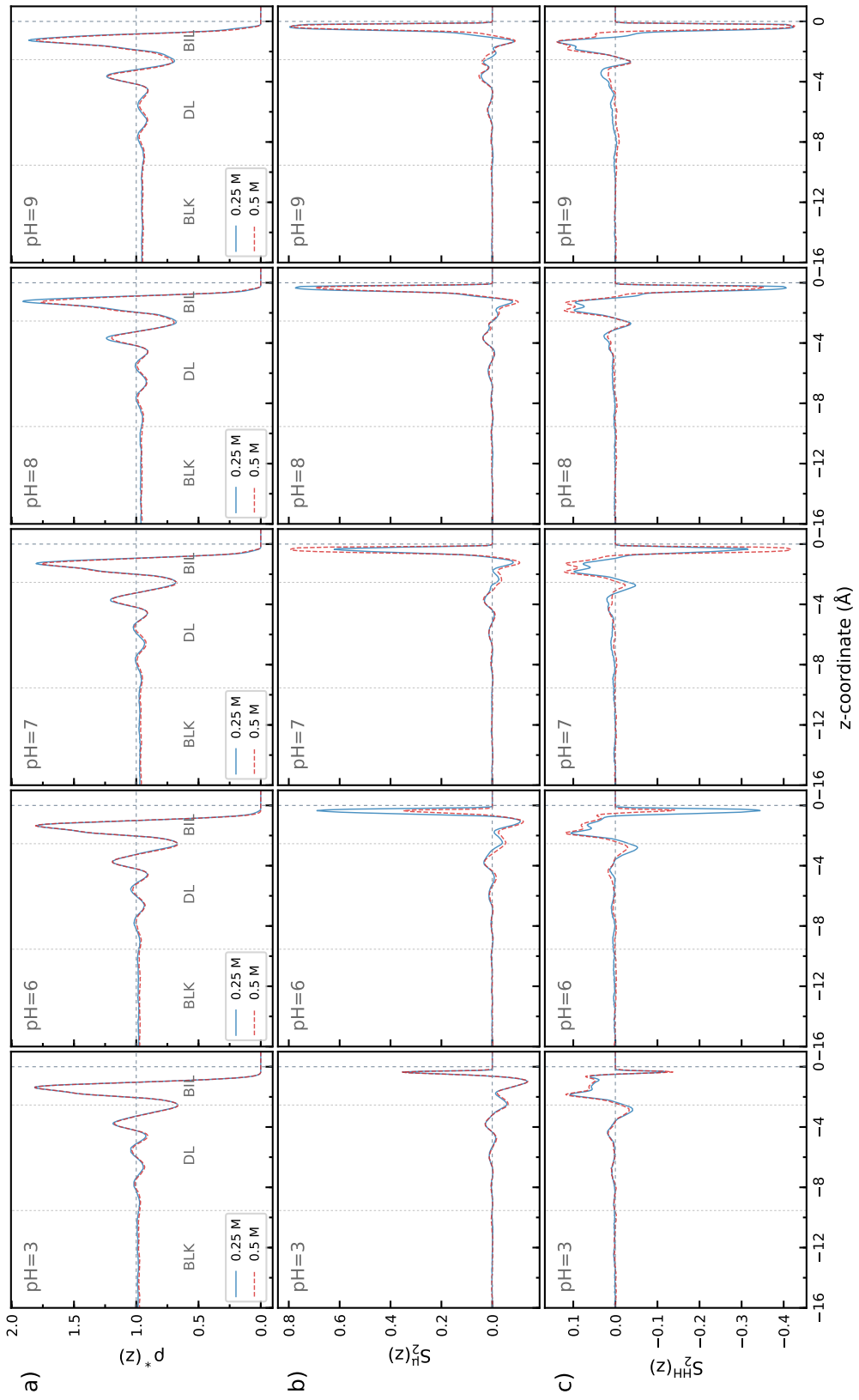

Figure S9: Axial profiles of the relative density $\rho^*(z)$ (a) and of the order parameters $S_2(z)$ for the dipole (b) and HH vector (c) of H_2O molecules at different pH values for the 0.25 M (full blue line) and 0.5 M (dashed red line) ionic strengths.

S2.8 z-profiles of ions distribution in all systems

Figure S10 presents the z-profiles of ion distribution in the interfacial region of all studied systems.

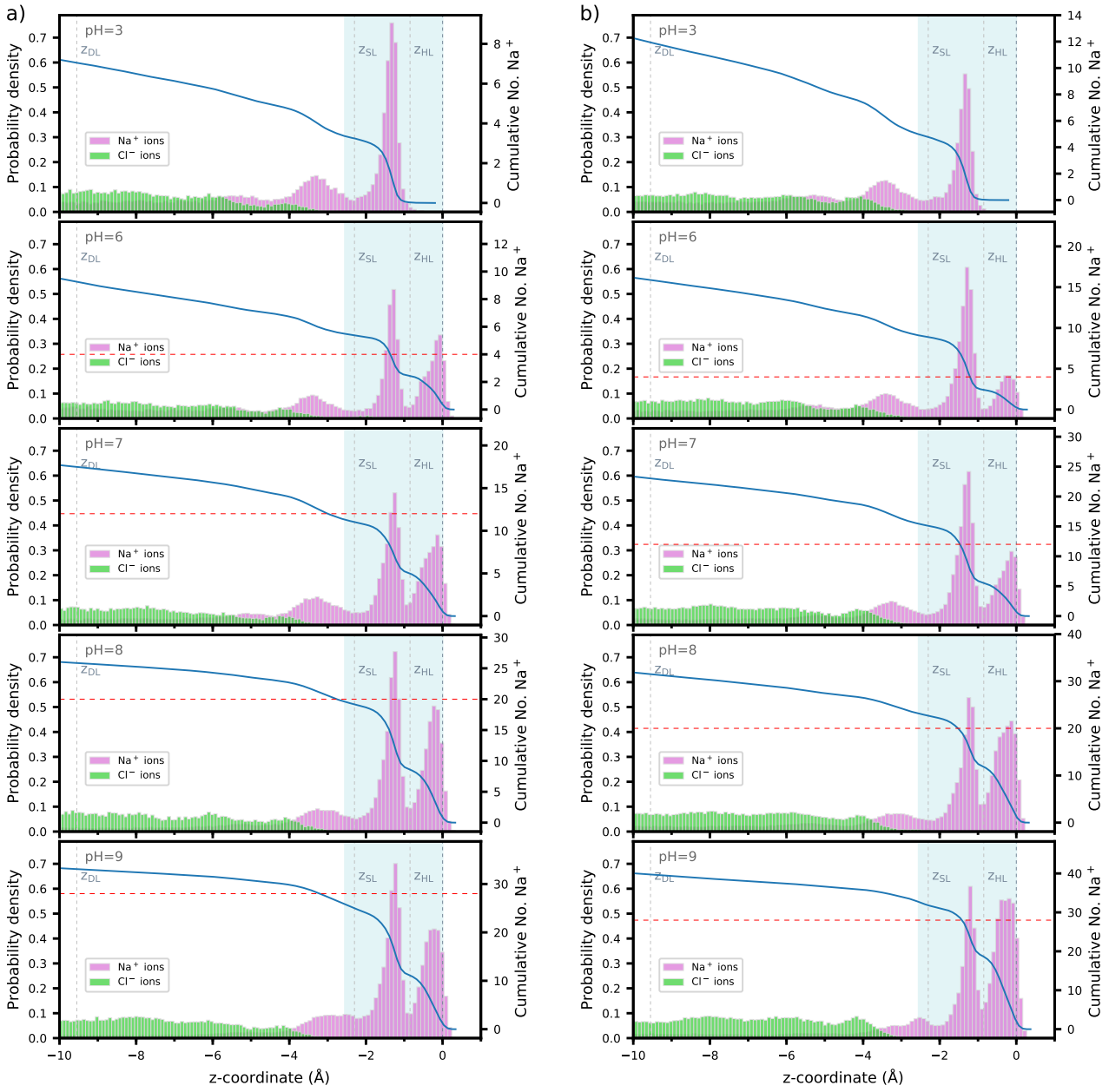

Figure S10: Histogram of ions distribution along the z-axis in the interfacial region at different pH values for the 0.25 M 3 (a) and 0.5 M (b) ionic strengths. The dashed vertical lines labeled z_{DL}, z_{SL} and z_{HL} indicate limits of the diffuse layer (DL), Stern layer (SL) and inner Helmholtz layer (HL), respectively. The shaded light blue zone denotes BIL, see Fig. S9 and the main article. The right-hand ordinate axis and blue line correspond to a cumulative number of cations as a function of distance from the surface. The red dashed line in the graphs indicates a number of cations needed to compensate the surface charge.

References

[1] Y. Wu, H. L. Tepper and G. A. Voth, *J. Chem. Phys.*, 2006, **124**, 024503.

[2] F. S. Emami, V. Puddu, R. J. Berry, V. Varshney, S. V. Patwardhan, C. C. Perry and H. Heinz, *Chem. Mater.*, 2014, **26**, 2647–2658.

[3] I. S. Joung and T. E. Cheatham, *J. Phys. Chem. B*, 2008, **112**, 9020–9041.

[4] A. P. Willard and D. Chandler, *J. Phys. Chem. B*, 2010, **114**, 1954–1958.

[5] S. Pezzotti, D. R. Galimberti, Y. R. Shen and M.-P. Gaigeot, *Phys. Chem. Chem. Phys.*, 2018, **20**, 5190–5199.

[6] D. Prada-Gracia, R. Shevchuk and F. Rao, *J. Chem. Phys.*, 2013, **139**, 084501.

[7] A. Morita and J. T. Hynes, *J. Phys. Chem. B*, 2002, **106**, 673–685.

[8] T. Ishiyama and A. Morita, *Chem. Phys. Lett.*, 2006, **431**, 78 – 82.

[9] T. Ishiyama and A. Morita, *J. Phys. Chem. C*, 2007, **111**, 738–748.

[10] Y. Nagata and S. Mukamel, *J. Am. Chem. Soc.*, 2011, **133**, 3276–3279.

[11] A. Morita, *J. Phys. Chem. B*, 2006, **110**, 3158–3163.

[12] R. W. Hellwarth, *Progress in Quantum Electronics*, 1977, **5**, 1–68.

[13] L. C. Geiger and B. M. Ladanyi, *Chem. Phys. Lett.*, 1989, **159**, 413–420.

[14] B. M. Ladanyi and Y. Q. Liang, *J. Chem. Phys.*, 1995, **103**, 6325–6332.

[15] S. Saito and I. Ohmine, *J. Chem. Phys.*, 1997, **106**, 4889–4893.

[16] T. Joutsuka, T. Hirano, M. Sprik and A. Morita, *Phys. Chem. Chem. Phys.*, 2018, **20**, 3040–3053.